Carcinogenesis, 2022, **XX**, 1–13
https://doi.org/10.1093/carcin/bgac032
Advance access publication 30 March 2022
Original Article

OXFORD

Original Article

Immunosuppressive tumor microenvironment in uterine serous carcinoma via CCL7 signal with myeloid-derived suppressor cells

Yuka Mise[1], Junzo Hamanishi[1], Takiko Daikoku[2], Shiro Takamatsu[1], Taito Miyamoto[1], Mana Taki[1], Koji Yamanoi[1], Ken Yamaguchi[1], Masayo Ukita[1], Naoki Horikawa[1], Kaoru Abiko[1], Ryusuke Murakami[1], Yoko Furutake[1], Yuko Hosoe[1], Jumpei Terakawa[2], Masahiro Kagabu[3], Tamotsu Sugai[4], Mitsumasa Osakabe[4], Hiroshi Fujiwara[5], Noriomi Matsumura[6], Masaki Mandai[1] and Tsukasa Baba[1,3,*]

[1]Department of Gynecology and Obstetrics, Kyoto University Graduate School of Medicine, Kyoto, Japan
[2]Institute for Experimental Animals, Advanced Science Research Center, Kanazawa University, Kanazawa, Japan
[3]Department of Obstetrics and Gynecology, Iwate Medical University School of Medicine, Shiwa, Japan
[4]Department of Diagnostic Pathology, Iwate Medical University School of Medicine, Shiwa, Japan
[5]Department of Obstetrics and Gynecology, Kanazawa University Graduate School of Medical Science, Kanazawa, Japan
[6]Department of Obstetrics and Gynecology, Kindai University School of Medicine, Sayama, Japan

*To whom correspondence should be addressed. Department of Obstetrics and Gynecology, Iwate Medical University School of Medicine, 2-1-1 Idaidori, Yahaba-cho, Shiwa, Iwate 028-3695, Japan. Tel: +81 19 613 7111; Fax; +81 19 622 1900; Email: babatsu@iwate-med.ac.jp

Abstract

Serous carcinoma of the uterus (USC) is a pathological subtype of high-grade endometrial cancers, with no effective treatment for advanced cases. Since such refractory tumors frequently harbor antitumor immune tolerance, many immunotherapies have been investigated for various malignant tumors using immuno-competent animal models mimicking their local immunities. In this study, we established an orthotopic mouse model of high-grade endometrial cancer and evaluated the local tumor immunity to explore the efficacy of immunotherapies against USC. A multivariate analysis of 62 human USC cases revealed that the tumor-infiltrating cell status, few CD8+ cells and abundant myeloid-derived suppressor cells (MDSCs), was an independent prognostic factor ($P < 0.005$). A murine endometrial cancer cell (mECC) was obtained from C57BL/6 mice via endometrium-specific deletion of *Pten* and *Tp53*, and another high-grade cell (HPmECC) was established by further overexpressing *Myc* in mECCs. HPmECCs exhibited higher capacities of migration and anchorage-independent proliferation than mECCs ($P < 0.01$, $P < 0.0001$), and when both types of cells were inoculated into the uterus of C57BL/6 mice, the prognosis of mice bearing HPmECC-derived tumors was significantly poorer ($P < 0.001$). Histopathological analysis of HPmECC orthotopic tumors showed serous carcinoma-like features with prominent tumor infiltration of MDSCs ($P < 0.05$), and anti-Gr-1 antibody treatment significantly prolonged the prognosis of HPmECC-derived tumor-bearing mice ($P < 0.05$). High CCL7 expression was observed in human USC and HPmECC, and MDSCs migration was promoted in a CCL7 concentration-dependent manner. These results indicate that antitumor immunity is suppressed in USC due to increased number of tumor-infiltrating MDSCs via CCL signal.

Graphical Abstract

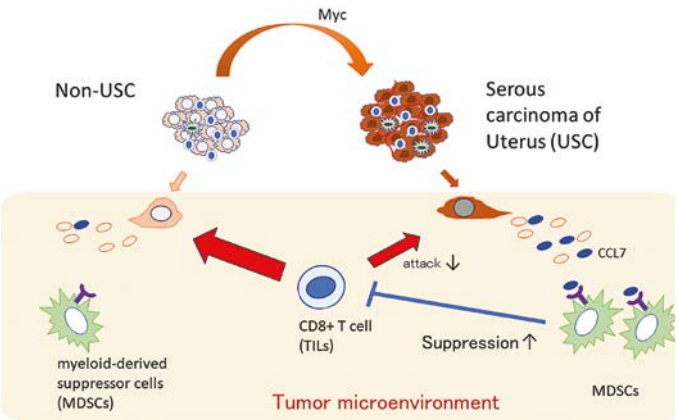

Abbreviations: CCL7, C-C motif chemokine 7; MDSC, myeloid-derived suppressor cell; TCGA, The Cancer Genome Atlas; USC, uterine serous carcinoma

Received: October 17, 2021; Revised: February 14 2022; Accepted: March 28, 2022

Introduction

Endometrial cancer is the most common gynecological malignancy (1). Although the prognosis is relatively good, patients with metastasis have a poor 5-year survival rate of less than 50% (2). Among the subtypes, uterine serous carcinoma (USC) is one of the non-endometrioid histological subtypes with a high risk of metastasis, accounting for 10% of all uterine cancers (3). Moreover, USC accounts for approximately half of all patients who die of endometrial cancer due to its resistance to currently available chemotherapy and the lack of effective treatment for advanced or recurrent cases (4). Therefore, it is necessary to develop novel effective treatments for USC.

Recent cancer genome analyses have shown that USC has a distinctive gene expression profile, including *p53* mutations and amplification of *PIK3CA* and *Myc* from the initiation of carcinogenesis, but the genes responsible for the true malignant characteristics of USC remain unclear (5–7). Through comprehensive gene expression analysis and *in vitro*/ *in vivo* studies, we have investigated the molecules involved in the resistance of USC to treatment and found that nuclear phosphorylation of serine residues of the STAT1 molecule, expressed in tumors, was responsible for platinum resistance of USC and the combination of CK2 inhibitors could attenuate this platinum resistance (8–11). Moreover, it is known that not only the characteristics of these cancer cells themselves but also their immune status in the cancer microenvironment are closely involved in the malignant traits of cancer (12). However, few reports have revealed the precise immune status of USC so far (13).

We have previously reported that in ovarian high-grade serous carcinoma (HGSC), the tumor microenvironment is in a state of antitumor immune tolerance and examined the potent efficacy of immune checkpoint inhibitors for overcoming chemo-resistance by altering the immune tolerant state (14–18). In USC, tumor stromal infiltration of CD8+ T cells was found to be not prominent at the tumor invasive frontier, suggesting that the tumor microenvironment of USC is also in a state of antitumor immune tolerance (10). It is, however, difficult to expect the existing immune checkpoint inhibitors (ICIs) alone to restore antitumor immune status because of the rarity of highly microsatellite instable (MSI-H) cases and low tumor mutational burden in USC (19–21). In ovarian HGSCs where MSI-H cases are not so common as well, intratumoral migration of myeloid-derived suppressor cells (MDSCs) apart from the PD-1/PD-L1 pathway was shown to suppress the intratumoral infiltration of CD8+ T cells, and it is reasonably expected that USC also employs these mechanisms to hinder the intratumoral infiltration of CD8+ T cells (22). Although an adequate immune-competent *in vivo* evaluation system is indispensable for developing novel antitumor immunotherapies, there have been no such immune-competent mouse models that match the pathogenesis of USC, which might be one of the reasons why we have not been able to develop effective therapies for USC (23).

In this study, an immune-competent allogeneic USC mouse model was generated to evaluate the antitumor immunity in the tumor microenvironment of USC. In addition, a novel therapeutic approach to attenuate MDSC migration was explored using this USC mouse model for improving the poor prognosis of USC.

Materials and methods

Clinical specimens of patients with USC

Surgical specimens from 62 patients with USC who underwent primary surgery at Kyoto University Hospital or Iwate Medical University Hospital between 2000 and 2019 were collected. The relevant clinical data were retrospectively reviewed under the approvals of the Ethical Committees of Kyoto University and Iwate Medical University.

Murine *in vivo* assays

Uterine epithelial cells were isolated from 4 weeks old C57BL/6 background $Pten^{ff}/p53^{ff}/PR^{Cre/+}$ mice, and the mouse endometrial cancer cell (mECC) was established as previously described (24). mECCs were transfected with two different vectors, mouse Myc-WT (Riken DNA bank, RDB_14100) or mouse Myc-DN (Riken DNA bank, RDB_14101) containing CAG promotor for establishing highly progressive cells (HPmECCs). HPmECCs or mECCs were inoculated intradermally into the right flank or injected into the right uterine horn of 6–8 weeks old female C57BL/6 mice. Anti-Ly6G/Ly6C antibody (clone NIMP-R14, BioXcell, Cat#BE0320, RRID:AB_2819047, Lebanon, NH) or rat IgG2b (clone LTF-2, BioXcell, Cat#BP0090, RRID:AB_1107780) treatment was initiated 4 days after tumor cell inoculation by administering 200 μg/body intraperitoneally every 48 h as recommended by the manufacturer. The intradermal tumor size was calculated as follows: volume = LD × SD^2 × 0.5, where LD is the long diameter (mm) and SD is the short diameter of the tumor (mm). Cages of mice were allocated to experimental groups by random draw. The investigator was not blinded to the group allocation. All animal studies were approved by the Kyoto University Animal Research Committee.

Immunohistochemical analysis

Formalin-fixed, paraffin embedded sections of the human clinical samples and mice tumor sections were stained with mouse anti-CD8 monoclonal (clone C8/144B; Nichirei Biosciences, Tokyo, Japan), mouse anti-CD33 monoclonal (clone PWS44; Leica Biosystems, Cat#PA0558, RRID:AB_10555285, Nussloch, Germany), rabbit anti-CD8 monoclonal (clone EPR20305; Abcam, Cat#ab209775, RRID:AB_2860566, Cambridge, UK), rat anti-Ly6G monoclonal (clone RB6-8C5; Abcam, Cat#ab25377, RRID:AB_470492), rat anti-Ly6C monoclonal (clone ER-MP20; Abcam, Cat#ab15627, RRID:AB_302004), rabbit anti-Granzyme B monoclonal (clone EPR22645-206; Abcam, Cat#ab255598, RRID:AB_2860567), rabbit anti-CD31 monoclonal (clone D8V9E; Cell Signaling technology, Cat#77699, RRID:AB_2722705) or rabbit anti-Ki67 monoclonal (clone SP6; Abcam, Cat#ab16667, RRID:AB_302459) antibodies and the average number of cells positive for these markers were calculated as described previously (23).

RNA extraction and real-time quantitative PCR

Total RNA was extracted from cells and freshly harvested tissues using Allprotect Tissue Reagent, RNeasy Mini Kit and Micro Kit (Qiagen, Hilden, Germany). cDNA was synthesized and amplified by RT-PCR using Rever Tra Ace qPCR RT Kit (TOYOBO, Osaka, Japan), Power Up SYBR Green Master Mix (Thermo Fisher Scientific Baltics, Vilnius, Lithuania), and a StepOne Plus real-time PCR system (Applied Biosystems,

MA). Relative target gene expression was estimated by dividing the threshold cycle (CT) value of the target gene by the CT value of the reference gene mRNA.

Protein extraction assay

Lysed cellular proteins were separated and transferred onto nitrocellulose membranes. Membranes were immunoblotted with the following antibodies: rabbit anti-cMyc antibody (Abcam, Cat#ab32072, RRID: AB_731658) and rabbit anti-GAPDH antibody (Cell Signaling Technology, Cat#2118, RRID: AB_561053). The bands were visualized using Molecular Image Gel DocTMXR+ and ChemiDocTMXRS+ Systems and quantitated using Image Lab 2.0 Software (Bio-Rad). MCP-3 (CCL7) protein levels in culture supernatants were measured using the mouse MCP-3 Instant ELISA Kit (Invitrogen; Vienna; Austria, abcam; ab205571).

CCL7 silencing

CCL7-specific siRNAs (Sigma Aldrich, St Louis, MO) were transfected into cells using Lipofectamine 2000 (Life Technologies, Carlsbad, CA). The sequence information of the siRNAs and primers used for Ccl7 mRNA expression analysis was described in Supplementary Table 1, available at *Carcinogenesis* Online.

In vitro functional assays

Cell proliferation was assessed by counting viable cells using Cell count Reagent SF (Nacalai Tesque), and the proliferation rate was plotted as described previously (23). For observing cell proliferation under a microscope, HPmECCs or mECCs seeded on glass slides were permeabilized and sequentially incubated with rabbit anti-Ki67 monoclonal antibody (clone SP6, Abcam) and secondary antibody, goat antirabbit IgG H&L (Alexa Fluor 647) (Abcam, Cat#ab150079, RRID:AB_2722623). Cell migration was assessed by capturing images at 0, 5 and 7 h after creating a mechanical wound on confluently grown cells in 6-well plates. Soft agar colony formation assay was performed as previously described (25). A single-cell suspension of HPmECCs or mECCs was stained using Annexin V Apoptosis Detection Kit I (BD Pharmingen, San Diego, CA) for analyzing the rate of apoptotic cells by flow cytometry.

Flow cytometry

Murine samples of spleen tissues, lymph nodes and tumors were collected and prepared as previously described (23). Cells were stained with the following antibodies: antimouse CD3 (clone 17A2, BioLegend, Cat#100221, RRID:AB_2057374), antimouse CD4 (clone GK1.5, Miltenyi Biotec, Cat#130-121-131, RRID:AB_2752219), antimouse CD8a (clone 53-6.7, BioLegend, Cat#100712, RRID:AB_312751), antimouse CD45 (clone 30-F11, BioLegend, Cat#103108, RRID:AB_312973, BD Biosciences, Cat#557659, RRID:AB_396774), antimouse F4/80 (clone BM8, BioLegend, Cat#123115, RRID:AB_893493), antimouse CD11b (clone M1/70, Miltenyi Biotec, Cat# 130-097-585, RRID:AB_2660136), antimouse Gr-1 (clone RB6-8C5, TONBO, San Diego, CA), antimouse Ly6C (clone HK1.4, BioLegend, Cat#128006, RRID:AB_1186135). Data was acquired using MACS Quant flow cytometer (Miltenyl Biotec, Bergisch Galdbach, Germany) and analyzed using FlowJo software (FlowJo, RRID:SCR_008520).

MDSC suppression assay

Gr-1+cells and T cells were isolated from mice orthotopic tumors and splenocytes using Easy Sep Mouse PE Positive Selection Kit and T cell Isolation Kit (STEMCELL Technologies). Sorted MDSCs were added to Carboxyfluorescein succinimidyl ester labeled T cells at different ratios and T cell proliferation was evaluated by flow cytometry.

Chemotaxis assay

MDSCs were generated as previously described (26). MDSCs were plated in the upper compartment, and conditioned medium of HPmECCs or mECCs or mouse recombinant CCL7 (Biolegend) was added in the lower compartment, and the number of MDSCs in the lower compartment was counted after 50 min of incubation (27).

RNA sequencing

Total RNA of HPmECCs, mECCs and cultured primary endometrial epithelial cells of C57BL/6 mice was extracted. Sequencing was performed on an Illumina Novaseq 6000 platform as a 100 base pair Paired-End reads. Adapter and low-quality sequence reads were removed from raw Fastq files using the Trim Galore tool (Trim Galore, RRID:SCR_011847) (28). The trimmed reads were aligned to the mouse reference genome (GRCm38) using STAR v2.6.1a(STAR, RRID:SCR_015899) and read counts and quantified gene expression values were calculated using RSEM v1.3.1 (RSEM, RRID:SCR_013027) as fragments per kilobase of transcript per million reads (FPKM) (29,30).

Statistics

Data are presented as the mean ± standard deviation (SD). All statistical analysis were performed using GraphPad Prism 7 (GraphPad Prism, RRID:SCR_002798). A P value of less than 0.05 was consisted statistically significant.

Results

Local antitumor immune microenvironment and genetics of human uterine serous carcinoma

A clinicopathological analysis for overall survival of 62 patients who underwent treatment for USC at Kyoto University Hospital and Iwate Medical University Hospital is shown in Table 1. Of the 62 patients, 34 were 65 years or older, 33 were at stage III/IV and 27 had recurrence. Recurrence was frequent in late-stage, positive ascites cytology, ≥50% myometrial invasion and lymphovascular invasion. Immunostaining for CD8 and CD33 was performed for these 62 patient samples, and the number of positive cells in the tumor microenvironment of each sample was assessed. There were more recurrence-free cases in cases with increased number of CD8+ cells (>25/HPF, $P < 0.005$, Fisher's exact test). On the other hand, in approximately one-third of USC samples, increased number of CD33+ cells were frequently observed in the tumor stromal area compared with the number of CD8+ cells (Supplementary Figure 1A, available at *Carcinogenesis* Online). Then, focusing on the number of CD8+ and CD33+ cells, the standardized variables were calculated, and a survival analysis was performed by classifying the 62 patients with USC into four groups based on zero for the standardized variables of CD8+ and CD33+ cells (Supplementary Figure 1B, available at *Carcinogenesis*

Table 1. Clinical analysis of human uterine serous carcinoma (USC)

Characteristics	Number of patients (ratio)	Univariate analysis		Multivariate analysis	
		HR (95%CI)	*P* value	HR (95%CI)	*P* value
Age					
<65	28 (45.2%)	1		1	
≥65	34 (54.8%)	0.83 (0.35–1.97)	0.68	1.24 (0.43–3.61)	0.69
FIGO stage					
I	28 (45.2%)	1		1	
II	1 (1.6%)				
III	27 (43.5%)	10.45 (2.42–45.17)	0.0017	5.22 (1.02–26.69)	0.047
IV	6 (9.7%)				
Myometrial invasion					
≤1/2	28 (45.2%)	1		1	
>1/2	34 (54.8%)	12.22 (2.83–52.82)	0.0008	5.07 (0.95–27.08)	0.058
Lymphovascular invasion					
+	29 (46.8%)	1		1	
-	33 (53.2%)	3.79 (1.45–9.86)	0.0064	3.07 (1.04–9.04)	0.041
Ascites					
–	37 (59.7%)	1		1	
+	24 (38.7%)	2.11 (0.86–5.18)	0.1	0.96 (0.35–2.69)	0.95
Not evaluated	1 (1.6%)				
$CD8_{low}CD33_{high}$					
–	50 (80.6%)	1		1	
+	12 (19.4%)	3.06 (1.18–7.91)	0.02	4.33 (1.28–14.58)	0.018

Univariate and multivariate analyses for overall survival of 62 USC cases based on six factors.$CD8_{low}CD33_{high}$ was designated using cut-off values: CD8+ cells ≤6.8/HPF, CD33+ cells ≥7.2/HPF. HR: hazard ratio, CI: confidence interval.

Online). Among the four groups, progression-free survival was worst in the $CD8_{V<0}CD33_{V\geq 0}$ group ($P < 0.05$, Gehan-Breslow-Wilcoxon test, Supplementary Figure 1C, available at *Carcinogenesis* Online). A multivariate Cox proportional hazard regression analysis revealed that $CD8_{low}CD33_{high}$ was an independent prognostic factor contributing to survival in USC (hazard ratio (HR) 4.33; 95% confidence interval (CI) 1.28–14.58; $P < 0.05$, Table 1) and HRs were also significant in stage III/IV (5.22; 95%CI 1.02–26.69; $P < 0.05$) and lymphovascular invasion (3.07; 95%CI 1.04–9.04; $P < 0.05$).

Single sample gene set enrichment analysis (ssGSEA) of endometrial cancer dataset from The Cancer Genome Atlas (TCGA) showed that myc signatures were more significantly enriched in USC than in normal endometrium and endometrioid carcinoma (Supplementary Figure 2A, available at *Carcinogenesis* Online). Among all cases of endometrial cancer subtypes in TCGA dataset, cases with high MYC expression showed significantly shorter disease-free survival than those with low expression ($P = 0.005$, Log-rank test, Supplementary Figure 2B, available at *Carcinogenesis* Online). Moreover, in cases with USC alone, MYC expression was significantly higher in patients with progression ($P < 0.05$, Mann–Whitney test, Supplementary Figure 2C, available at *Carcinogenesis* Online).

Establishment of a highly progressive mouse endometrial cancer model

Endometrium-specific Cre-Lox deletion of both *Pten* and *Tp53* via regulation of the progesterone receptor promoter is known to generate a spontaneous carcinogenic mouse model of endometrial cancer (31). Since this hybrid mouse strain cannot be evaluated for antitumor immunity, a mouse endometrial cancer cell, mECC, was established from the uterine carcinoma tumor tissue of its pure strain model generated by backcrossing in C57BL/6 mice (24). Orthotopic mECC tumors inoculated into the uterus exhibited marked calcifications and lacked mitosis and nuclear atypia, which is designated as pathologically not characteristic of high-grade carcinoma (Supplementary Figure 3A, available at *Carcinogenesis* Online).

Then, a high-grade endometrial cancer cell (Highly Progressive mECC: HPmECC) was established by further introducing c-Myc in mECCs (Supplementary Figure 3B, available at *Carcinogenesis* Online). RNA sequencing analysis was performed using cultured HPmECCs and mECCs, as well as primary cultured C57BL/6 normal endometrial cells for assessing the genetic characteristics of HPmECCs. Using various myc signatures and genes significantly elevated in USC compared with normal endometrium in TCGA dataset, ssGSEA scores were calculated for these three types of cells. We observed that high-grade endometrial cancer-like scores were higher in the order of HPmECC, mECC and normal endometrium (Supplementary Figure 3C, available at *Carcinogenesis* Online).

To investigate the proliferative potential of HPmECCs and mECCs *in vitro*, Ki67 immunofluorescence staining and WST-1 assay were performed. The number of Ki67-positive cells was significantly lower in HPmECCs ($P < 0.0005$, Mann–Whitney test, Figure 1A and B). However, there was no difference in

cell viability and cell doubling time (Supplementary Figure 3D, available at *Carcinogenesis* Online), and the number of apoptotic cells was significantly lower in HPmECCs compared with mECCs ($P < 0.01$, Mann–Whitney test, Figure 1C and D).

Next, wound healing assay was performed to evaluate the cell migrating ability of these cells. The results showed significantly higher cell migration of HPmECCs ($P < 0.05$ after 5 h and $P < 0.01$ after 7 h, Mann–Whitney test, Figure 1E and F). Furthermore, in the soft agar colony formation assay, while mECCs did not form colonies, HPmECCs formed colonies ($P < 0.0001$, Mann–Whitney test, Figure 1G and H).

HPmECC-derived orthotopic tumors in immuno-competent mice

To assess the *in vivo* tumor growth capability under antitumor immunity, orthotopic tumor models using immuno-competent mice were established. Tumor formation was slow when mECCs were inoculated into the uterine horns of C57BL/6 mice, but in mice orthotopically inoculated with HPmECCs, tumors larger than 5 mm in diameter were confirmed by ultrasonography 13 days after inoculation (Supplementary Figure 4A, available at *Carcinogenesis* Online). HPmECC-derived orthotopic tumors exhibited solid growth (Figure 2A) as well as characteristics of high-grade tumors with marked mitosis, nuclear atypia and vascular invasion (Figure 2B–F). We examined the *in vivo* proliferative capacity, and Ki67-positive cells were observed more frequently in HPmECC-derived tumors ($P < 0.05$, Mann–Whitney test, Figure 2G and H), and subcutaneous tumor growth rate was also faster ($P < 0.0005$ at day13, $P < 0.0001$ at day17, Mann–Whitney test, Figure 2I). In addition, the overall survival of HPmECC-derived orthotopic carcinoma-bearing mice was significantly shorter than that of mECC-derived orthotopic carcinoma-bearing mice ($P < 0.001$, Log-rank test, Figure 2J).

Antitumor immune tolerant environment in HPmECC-derived orthotopic tumors

In order to evaluate the local antitumor immunity status, mECC-derived tumors were collected at 27 days after intrauterine administration and HPmECC-derived tumors at 13 days after intrauterine administration, when tumor growth was still localized in the uterus. To compare TILs in HPmECC- and mECC-derived orthotopic tumors, we first performed CD8 immunostaining. The number of CD8+ cells infiltrating into the tumors was low in both, and no significant difference was observed (Figure 3A and B). Then, flow cytometry was performed to evaluate the differences in CD8+ T cells in the spleen, lymph nodes and tumor tissues of HPmECC- and mECC-derived orthotopic tumors: the rate of CD45+CD3+CD8+ cells was significantly lower in the lymph nodes of mice inoculated with HPmECCs ($P < 0.005$, Mann–Whitney test, Figure 3C and D), whereas there was no difference in CD8+ cells in the spleen and tumor tissues between both mouse models (Supplementary Figure 4B, available at *Carcinogenesis* Online).

We then compared the function and number of MDSCs in HPmECC- and mECC-derived orthotopic tumors. MDSCs are characterized as CD11b+Gr-1+ cells in mice, and anti-Gr-1 mAbs recognize epitopes common to Ly6C and Ly6G. First, Gr-1+ cells collected from the respective tumors were co-cultured with activated T cells and subjected to immunostaining for Ly6G (G-MDSC marker) and Ly6C (M-MDSC marker). Gr-1+ cells from both types of tumors showed similar mitotic inhibitory effect on T cells (Supplementary Figure 4C, available at *Carcinogenesis* Online), and both Ly6G+ and Ly6C+ cells were abundant in HPmECC-derived tumors ($P < 0.05$, Mann–Whitney test, Figure 3E–G). Comparison of MDSCs between HPmECC- and mECC-derived orthotopic tumor-bearing mice was also performed by flow cytometry. There was a significantly higher proportion of Ly6G+ cells (G-MDSCs) and Ly6C+ cells (M-MDSCs) in both spleen and tumor tissues of mice inoculated with HPmECCs ($P < 0.05$, Mann Whitney test, Figure 3H–J).

Thereafter, the validity of MDSC removal treatment was assessed in HPmECC-derived orthotopic tumor-bearing mice. For excluding sex hormone-induced differences in tumor implantation, bilateral ovaries of C57BL/6 mice were pre-resected, and 1.0×10^6 HPmECCs were injected into the unilateral horn of the uterus. On day 2 after inoculation, anti Gr-1 antibody (BE0320) or IgG was administered intraperitoneally at 200 μg/body, and mice were euthanized on day 4 for MDSC analysis. MDSCs in the spleen were significantly decreased in the anti-Gr-1 antibody-treated group ($P < 0.01$, Welch's test, Figure 4A and B). To evaluate the therapeutic effect of BE0320, the same tumor-bearing mouse model was injected with 200 μg/body of BE0320 or IgG intraperitoneally every 48 h starting on day 4. The survival time was significantly prolonged in the BE0320-treated group ($P < 0.05$, Log-rank test, Figure 4C).

Regulation of MDSC migration in high-grade endometrial carcinoma

RNA sequencing of HPmECCs and mECCs to compare the expression of chemokines in each cell revealed that *Ccl2*, *Ccl20*, *Ccl3*, *Ccl5*, *Ccl7*, *Cxcl1* and *Cxcl10* were highly expressed in HPmECCs (Supplementary Table 2A, available at *Carcinogenesis* Online). Similarly, in a two-group comparison with C57BL/6 normal endometrial primary culture cells, *Ccl27a*, *Ccl5*, *Ccl7*, *Ccl9*, *Cxcl10*, *Cxcl12*, *Cxcl13* and *Cxcl15* were highly expressed in HPmECCs (Supplementary Table 2B, available at *Carcinogenesis* Online). Since *Ccl5*, *Ccl7* and *Cxcl10* were highly expressed in HPmECCs, we assessed whether there were differences in the expression levels of *CCL5*, *CCL7* and *CXCL10* in each histological subtype of endometrial cancer patients among the TCGA dataset. *CCL7* expression was significantly higher in the patients with USC than in those with low-grade endometrioid carcinoma ($P < 0.0001$, one-way ANOVA, Supplementary Figure 5A, available at *Carcinogenesis* Online), and the prognosis of those with high *CCL7* expression was worse ($P < 0.05$, Log-rank test, Figure 5A).

In HPmECCs, *Ccl7* mRNA expression was higher and its concentration in the culture supernatant was also higher compared with mECCs ($P < 0.05$, <0.0001, *t*-test, Figure 5B and C). MDSCs added to HPmECC culture supernatants showed higher migration than mECC ($P < 0.05$, *t*-test, Figure 5D). To assess the chemotactic effect of CCL7 secreted by USC, *Ccl7* expression in HPmECCs was evaluated using five *Ccl7* siRNAs (Supplementary Figure 5B, available at *Carcinogenesis* Online). *Ccl7* mRNA expression and its secretion into the culture supernatant was significantly

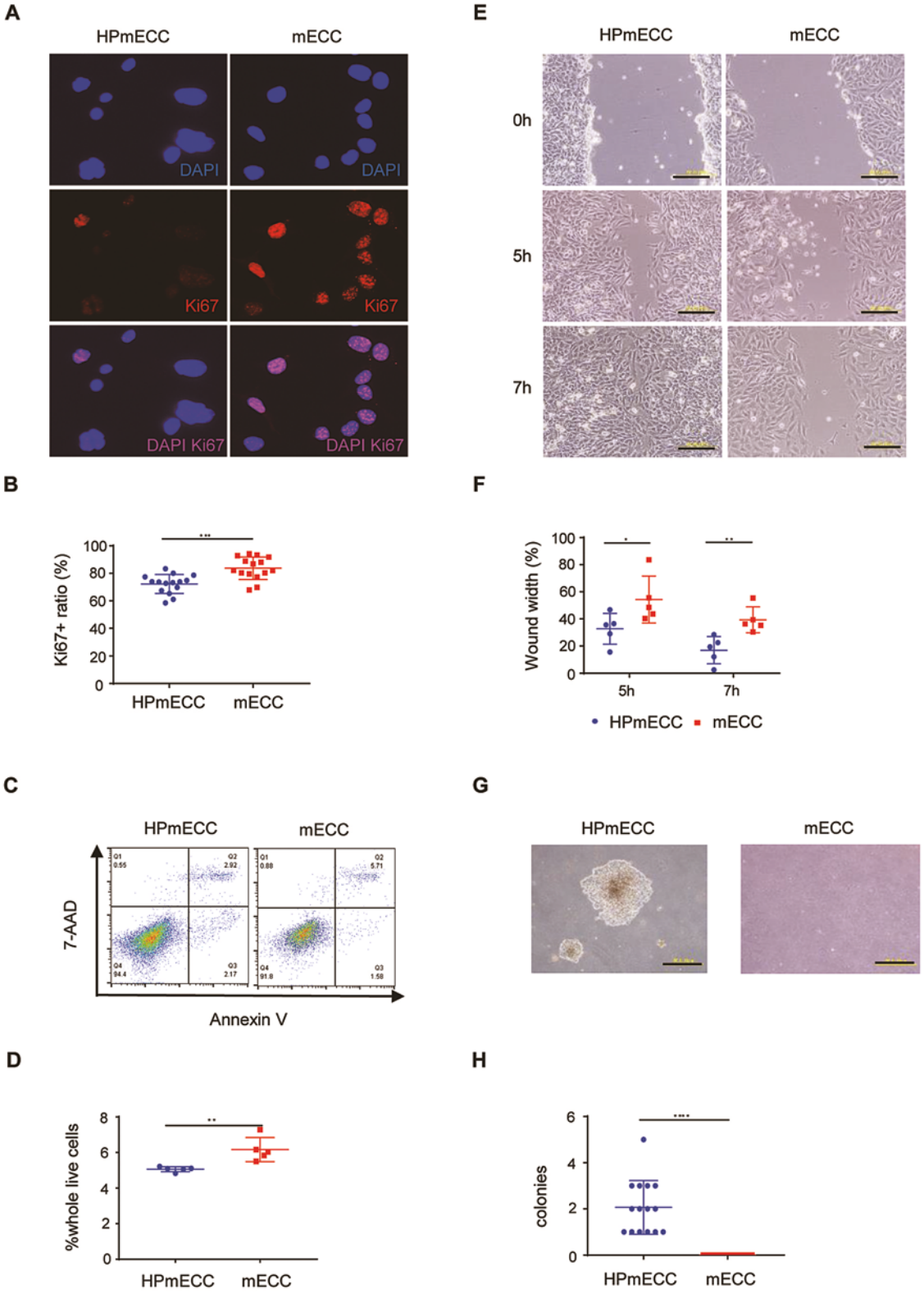

Figure 1. HPmECCs exhibit high survival capability. (**A** and **B**) Immunofluorescence staining of HPmECCs and mECCs to assess *in vitro* cell proliferation activity. Upper row: DAPI, middle row: Ki67 and bottom row: merged. Ki67+ cells were less frequent in HPmECCs than in mECCs *in vitro*. $n = 15$, $^{***}P = 0.0004$, Mann–Whitney test. (**C** and **D**) Flow cytometric analysis of HPmECCs and mECCs assessing *in vitro* apoptotic status. Cells were double-stained with Annexin V and 7-AAD. Increased number of apoptotic cells were observed in mECCs. $n = 5$, $^{**}P = 0.0079$, Mann–Whitney test. (**E** and **F**) Wound healing assay. (E) Representative images of HPmECCs and mECCs cultured for 0 h (upper row), 5 h (middle row) and 7 h (bottom row) after creating a scratch wound. Scale bar, 100 μm. (F) Comparison of residual wound width (μm) at 5 h (left) and 7 h (right) after scratch wound. $n = 5$, $^{*}P = 0.031$, $^{**}P = 0.0079$, Mann–Whitney test. (**G** and **H**) Soft agar colony formation assay. (G) Representative images of HPmECCs and mECCs cultured in soft agar for 3 weeks. (H) Comparison of colony numbers. $n = 15$, $^{****}P < 0.0001$, Mann–Whitney test. Averaged data are presented as the mean ± SD.

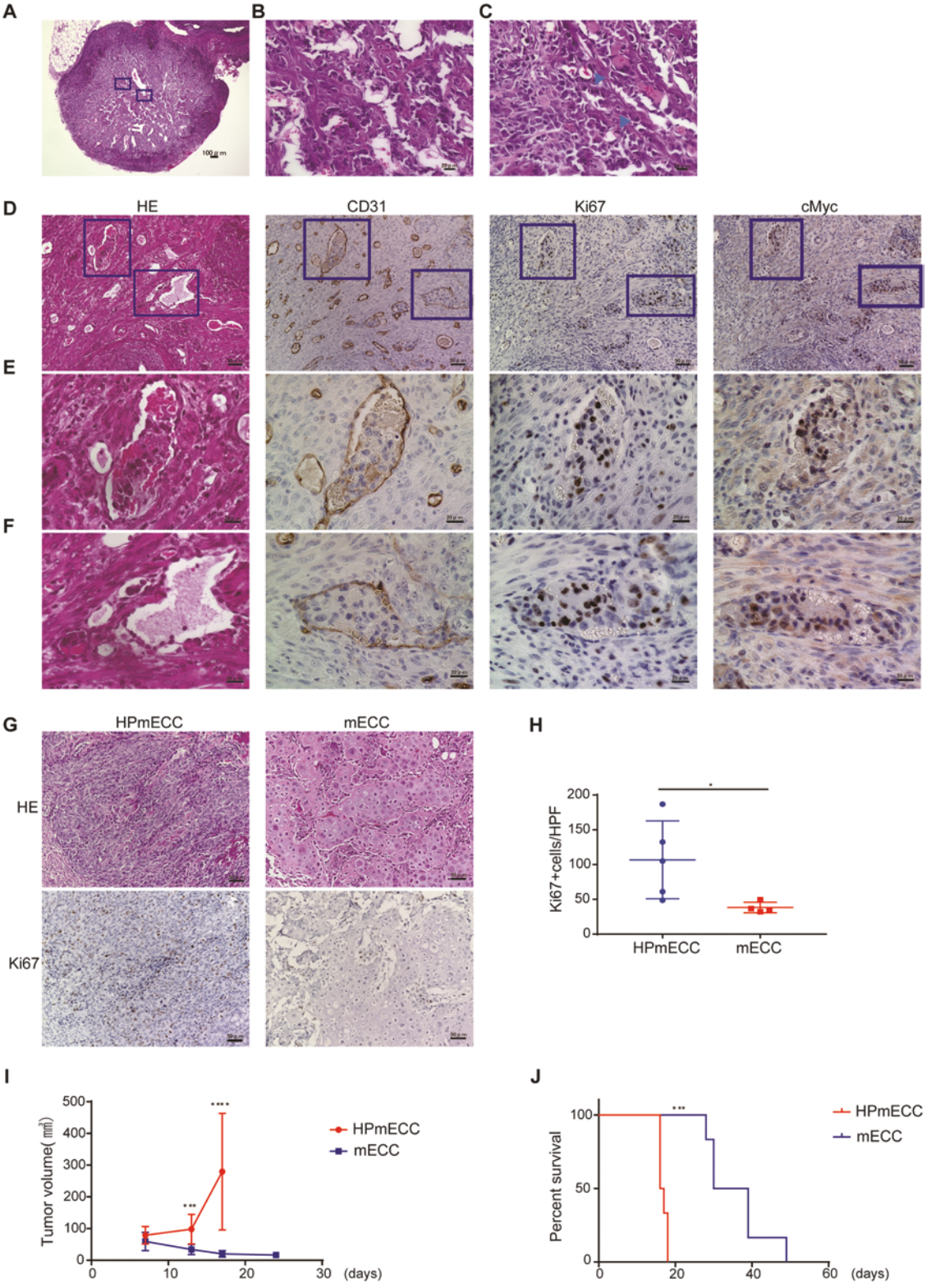

Figure 2. Histopathological features of HPmECC-derived tumors in immune-competent mice. (**A**–**F**) Pathological features of HPmECC-derived tumor inoculated into the uterus of C57BL/6 mice. Scale bars, A 100 μm, B–D 50 μm, E, F 20 μm. (A) Tumor gross image, ×40. Magnified images of (A), papillary structures (B, ×400) and mitosis (C, arrow head, ×400). (D) ×200, vascular space infiltration was indicated in rectangles (H&E, CD31, Ki67 and cMyc), (E, F) ×600. (**G** and **H**) *In vivo* proliferative ability of HPmECC- ($n = 5$) and mECC-derived ($n = 4$) tumors. (G) Representative images of H&E and Ki67 staining of inoculated tumors. Scale bars, 50 μm. (H) Comparison of the number of Ki67+ tumor cells. $^{*}P = 0.0317$, Mann–Whitney test. Averaged data are presented as the mean ± SD. (**I**) Tumor growth from subcutaneously inoculated HPmECC and mECCs. $n = 4$, $^{***}P = 0.0002$ (day 13), $^{****}P < 0.0001$ (day 17), Mann–Whitney test. (**J**) Survival analysis of C57BL/6 mice bearing HPmECC- or mECC-derived tumors in the uterus. $n = 6$, $^{***}P = 0.0007$, Log-rank test.

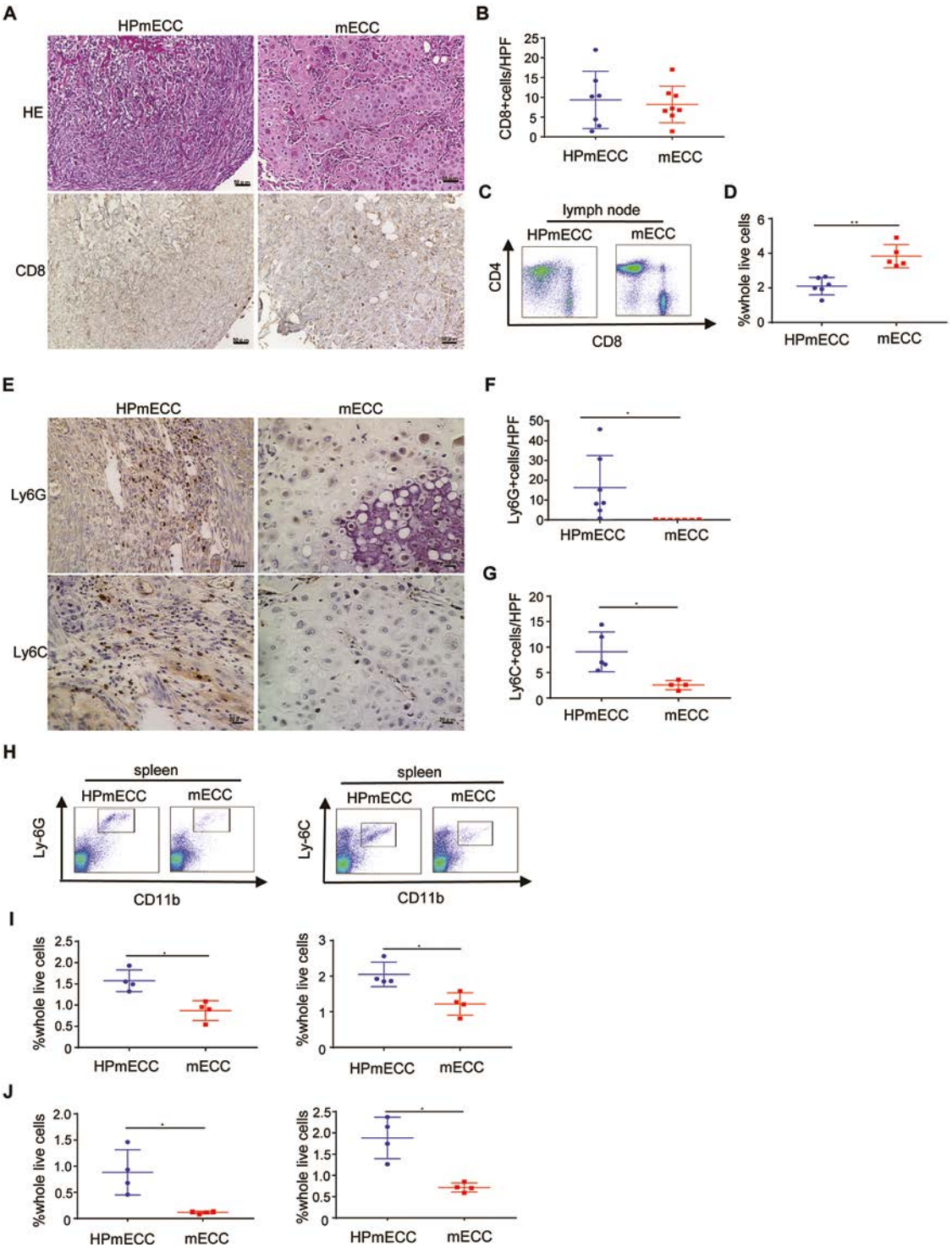

Figure 3. Immuno-profile of immune-competent mice bearing uterine HPmECC-derived tumors. (**A** and **B**) CD8+ cells in uterine inoculated tumors in C57BL/6 mice. Representative images of H&E and CD8 staining. ×200, scale bars, 50 μm (A). Comparison of the number of CD8+ cells (B, $n = 7, 8$). (**C** and **D**) Flow cytometric analysis of CD8+ cells in regional lymph nodes of C57BL/6 mice bearing uterine tumor. Representative cytometry images (C). The ratio of CD8+ cells/ whole cells was lower in mice inoculated with HPmECCs (D, $n = 6, 5$, $P = 0.0043$, Mann–Whitney test). (**E**–**G**) Ly6+ cells in uterine inoculated tumors in C57BL/6 mice. Representative images of Ly6G and Ly6C staining. ×400, scale bars, 20 μm (E). Comparison of the number of Ly6G+ cells (F, $n = 7$, $P = 0.038$) and Ly6C+ cells (G, $n = 5,4$, $P = 0.018$), Mann–Whitney test. (**H**–**J**) Flow cytometric analysis of CD11b+Ly6+ cells in the spleen and tumor of C57BL/6 mice bearing uterine tumor. (H) Representative cytometry images of the spleen. (I) Among whole spleen cells, the ratios of CD11b+Ly6G+ cells (left) and CD11b+Ly6C+ cells (right) were higher in mice inoculated with HPmECCs. $n = 4$, $^*P < 0.05$, Mann–Whitney test. (J) Among whole tumor cells, the ratios of CD11b+Ly6G+ cells (left) and CD11b+Ly6C+ cells (right) were higher in mice inoculated with HPmECCs. $n = 4$, $^*P < 0.05$, Mann–Whitney test. Averaged data are presented as the mean ± SD.

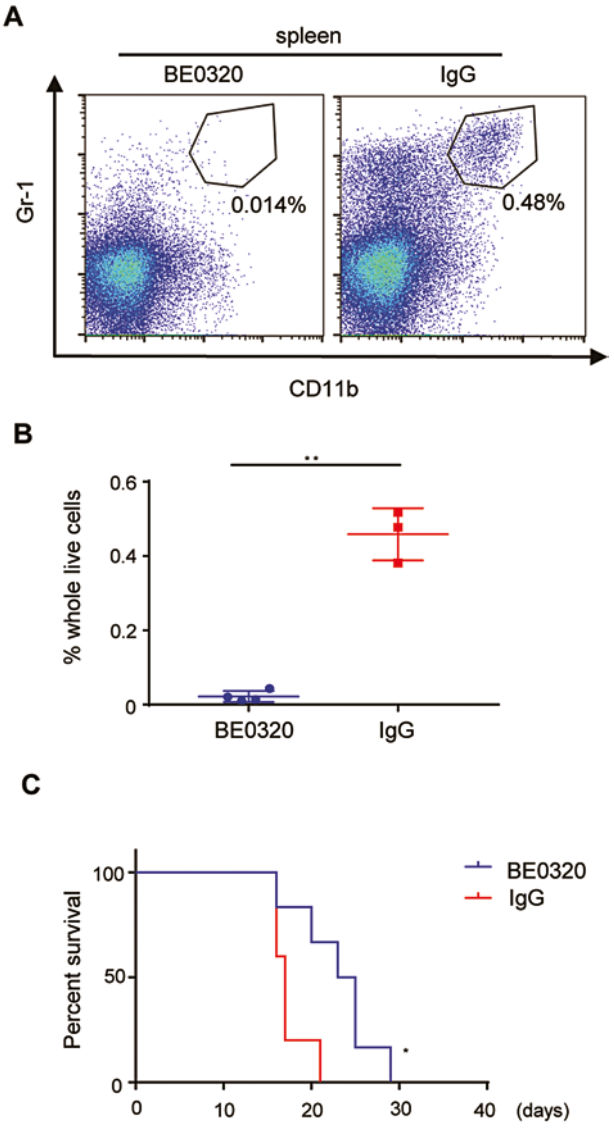

Figure 4. Survival analysis of HPmECC-derived tumor-bearing mice upon MDSC depletion. (**A** and **B**) Flow cytometric analysis of CD11b+Gr-1+ cells in the spleen of C57BL/6 mice bearing HPmECC-derived uterine tumor after the treatment of anti-Gr-1Ab (BE0320) or control IgG. (A) Representative cytometry images of spleen lysate treated with BE0320 (left) or control IgG (right). (B) CD11b+Gr-1+ cells were significantly depleted in BE0320-treated mice. $n = 4, 3$, $^{**}P = 0.0070$, Welch's test. Averaged data are presented as the mean ± SD. (**C**) Survival analysis of C57BL/6 mice bearing HPmECC-derived uterine tumor treated with BE0320 or control IgG. $n = 6, 5$, $^{*}P = 0.0269$, Log-rank test.

suppressed with two siRNAs ($P < 0.0005$, <0.0001, *t*-test, Figure 5E and F), and the number of migrating MDSCs was also reduced by *Ccl7* suppression (Figure 5G, Supplementary Figure 5C, available at *Carcinogenesis* Online). On the other hand, the number of migrating MDSCs was increased in a concentration-dependent manner upon addition of recombinant CCL7 ($P = 0.001$, one-way ANOVA, Figure 5H).

Finally, we assessed whether there was a correlation between CCL7 and CD33 in human USC samples by analyzing published datasets. In both TCGA and GSE56026 datasets, positive correlations were found between the expression of *CCL7* and *CD33* in USC (TCGA: $r = 0.4539$, $P < 0.0001$, GSE56026: $r = 0.6227$, $P < 0.05$, Figure 5I).

Discussion

Recent evidence indicates that several immune escape mechanisms play a major role in solid tumors that are resistant to conventional treatments. TCGA data analysis of endometrial cancer has shown an association between antitumor immune activity in the tumor microenvironment and prognosis, suggesting that cases with poor antitumor immune response have poorer prognosis (32). The ESTIMATE (Estimation of STromal and Immune cells in MAlignant Tumor tissues using Expression data) algorithm and scoring of the immune response showed that the average immunoreactivity score was lowest in the copy number high group, which indicated that there were many cases with low local tumor immunoreactivity in USC (33). Previous studies have reported that the prognosis of USC cases was different with or without STAT1 expression and there was a difference in the number of CD8+ T cells at the tumor invasive frontier (10,11). Therefore, it is supposed that antitumor immune status may be different among USCs depending on their individual genetic characteristics.

In the present study, immunostaining of 62 USC samples revealed that the prognosis was better in patients with more CD8+ cells infiltrating into the tumor, and worse in patients with more CD33+ cells resulting in local tumor immunosuppression. Since these results indicated that the local immune response is also prognostically relevant in USC and that attenuating antitumor immunosuppression may improve the prognosis of patients with USC, antitumor immune response of USC and an immune-therapeutic approach was investigated using an immune-competent *in vivo* evaluation system.

A mouse endometrial cancer cell (mECC) was established from a pure C57BL/6 (B6) mouse strain, and endometrium-specific depletion of *Pten* and *Trp53* resulted in endometrial cancer. However, the histopathological findings as well as the *in vivo* tumor-forming capacity of mECCs was too low to be considered as a high-grade endometrial cancer cell mimicking USC. TCGA data analysis of endometrial cancer indicated that a copy number high group, which mainly consists of USC and high-grade endometrioid carcinoma, was characterized by superimposed myc signaling, suppressed estrogen receptor signaling and aberrant p53 activity (5,6). In this TCGA cohort, myc signature of USC was significantly elevated compared with endometrioid carcinoma and the prognosis was significantly worse in cases with high MYC expression (10). Based on these findings, *c-Myc* was further introduced into mECCs to activate the myc pathway for obtaining a more malignant cell (HPmECC). These cells formed almost 100% orthotopic tumors in B6 mice within 2 weeks after uterine inoculation, and these orthotopic tumors histopathologically showed micropapillary glandular structures accompanied by lymphovascular infiltration and cytologically exhibited nuclear enlargement and atypia with frequent mitosis and abnormal mitotic figures. These pathological findings are similar to microscopic features observed in human USCs. Although the mitotic activity was not prominent in 2D culture, HPmECCs exhibited high growth potential in 3D culture as well as inoculated tumor growth in mice, which synchronicity represented the progressive nature of USC. And HPmECCs exhibited higher capacities of apoptosis-resistance and migration than mECCs, which was compatible with malignant *in vitro* phenotypes of USC. Considering these *in vivo* and *in vitro* results, HPmECCs and mECCs were respectively used as representative syngeneic high-grade endometrial carcinoma

cells mimicking USC, and its low-grade counterpart to investigate the antitumor immune status in immune-competent mice.

Assessment of the tumor microenvironment by immunostaining and flow cytometry indicated that HPmECC tumors exhibited a greater antitumor immunosuppressive status compared with mECC tumors. *Myc*, which is the oncogene that causes the differences between these cells in the current study, is reported to induce local antitumor immunosuppression and promote tumor growth via elevating the expression of PD-L1 and associated cytokines involved in immunosuppression (34,35). Thus, *Myc* targeting therapy has been long expected potent for suppressing both tumor progression and microenvironmental immune evasion (36). However, it is so far not launched in the clinical setting because myc signals are active in several normal tissues as well. Therefore, we focused on the actual tumor microenvironment where the antitumor immunity was attenuated although an intriguing report was recent published to imply the therapeutic potency of a selective myc inhibitor to recover antitumor immunity in *Myc* activated tumors (37). In this study, it was demonstrated that the survival of HPmECC-derived tumor-bearing B6 mice was prolonged by administration of anti-Gr-1 antibody to suppress the activity of MDSCs. It was a limitation of this study that intra-tumoral TILs analysis was not as satisfactory as MDSC number and function. Nevertheless, our result indicates that manipulating immunosuppressive status in the tumor microenvironment may play a significant role in the prognosis of patients with USC. Although the number of MDSCs in the tumor microenvironment can be assessed using tumor-bearing nude mice, the activity of local MDSCs and survival outcome were different irrespective of whether mouse ovarian cancer cells were transplanted into immunodeficient mice or allogeneic mice (23). Moreover, it is considered mandatory to employ immune-competent mouse models to evaluate the local antitumor immunity and to investigate experimental immunotherapies.

There have been three mice syngeneic carcinogenesis models reported in which endometrial cancer spontaneously arises through genetic manipulation (31,38,39). Although the local antitumor immunity is assessable using these models, it is difficult not only to conduct multiplicate assays but to replicate assays due to long breeding periods and non-negligibly large costs, and therefore not so suitable to develop and evaluate new treatments using these models. Another immunoreactive orthotopic mouse endometrial cancer model was recently reported, but it is regarded as not a true allogeneic mouse model since the cancer cell line was established via crossbreeding with several strains (39).

In this study, HPmECC was established via triple oncogenic manipulation, and not with double. In the mouse allogeneic HGSC model generated from intraperitoneal cells of B6 mice by deleting *Trp53* and overexpressing *AKT* and *c-Myc*, it was observed that mutations in only two of the three genes was insufficient to cause tumorigenesis, while mutations in all the three genes could overcome host immune surveillance resulting in orthotopic tumor formation (40). Since this model is suitable for assessing the antitumor immunity of patients bearing ovarian/tubal/peritoneal HGSC, B6 mice bearing HPmECC-derived tumors in the uteri are considered applicable as an allogeneic mouse model stably forming orthotopic tumor for evaluating the local tumor immunity and efficacy of new immunotherapies against USC.

Based on the current findings, intra-tumoral migration of MDSCs is thought to suppress the accumulation of CD8+ T cells resulting in therapeutic resistance of USC, but the mechanism causing the accumulation of MDSCs in the tumor was not well clarified for USC. Since it was demonstrated in ovarian HGSCs that CXCL1/2 promoted MDSC migration towards the tumor, there may exist a chemokine crosstalk in the tumor microenvironment between the tumor and MDSCs to attenuate antitumor immunity (23). In this study, RNA sequencing of human endometrial cancer samples and mouse models was performed to identify chemokines commonly and highly expressed in human USC and HPmECCs, and CCL7 was identified as a candidate for chemo-attractants of MDSCs. While it was shown that CCL7 significantly increases MDSC migration, in this USC experimental setting, the specific receptor for CCL7, similar to CXCR2 for CXCL1/2, was not identified in MDSCs (23). Regarding the role of CCL7 in tumor biology, while its involvement in tumor metastasis has been mainly featured, its function in MDSC migration is unclear (41). These are the limitations of this study that needs to be further investigated. However, CCR2, a potential receptor for CCL7, is known to be involved in the migration of tumor-associated macrophages (TAMs) (42,43). Furthermore, it was recently described that recruitment of MDSCs to lymph nodes draining the tumor, where efficient priming of antitumor T cells mainly occurs, was mediated via CCR2-cytokines dependent pathway to inhibit T-cell activation (44–46). Thus, MDSC-specific CCL7-CCR2 inhibition along with standard treatment may overcome antitumor immune tolerance of USC to improve the current miserable prognosis of USC patients

In conclusion, our results showed that depletion of MDSCs prolonged the survival of murine high-grade endometrial tumor-bearing mice, and that CCL7 secreted by USC might promote intra-tumoral MDSC migration. Although further analysis is needed, targeting of chemokine-mediated MDSC migration into the tumor would potentially improve the poor prognosis of USC.

Supplementary material

Supplementary data are available at *Carcinogenesis* online.

Funding

This work was supported by Grants-in-Aid for Strategic Medical Science Research (18K09287, 20H03822) from the Ministry of Education Culture, Sports, Science, and Technology of Japan.

Acknowledgements

We would like to thank Editage (www.editage.com) for English language editing.

Conflict of Interest Statement

None declared.

Authors' contributions

Y.M., J.H. and T.B. contributed to study conception, study design, quality control of data, data analysis, interpretation and manuscript preparation. T.D. and A.M. contributed

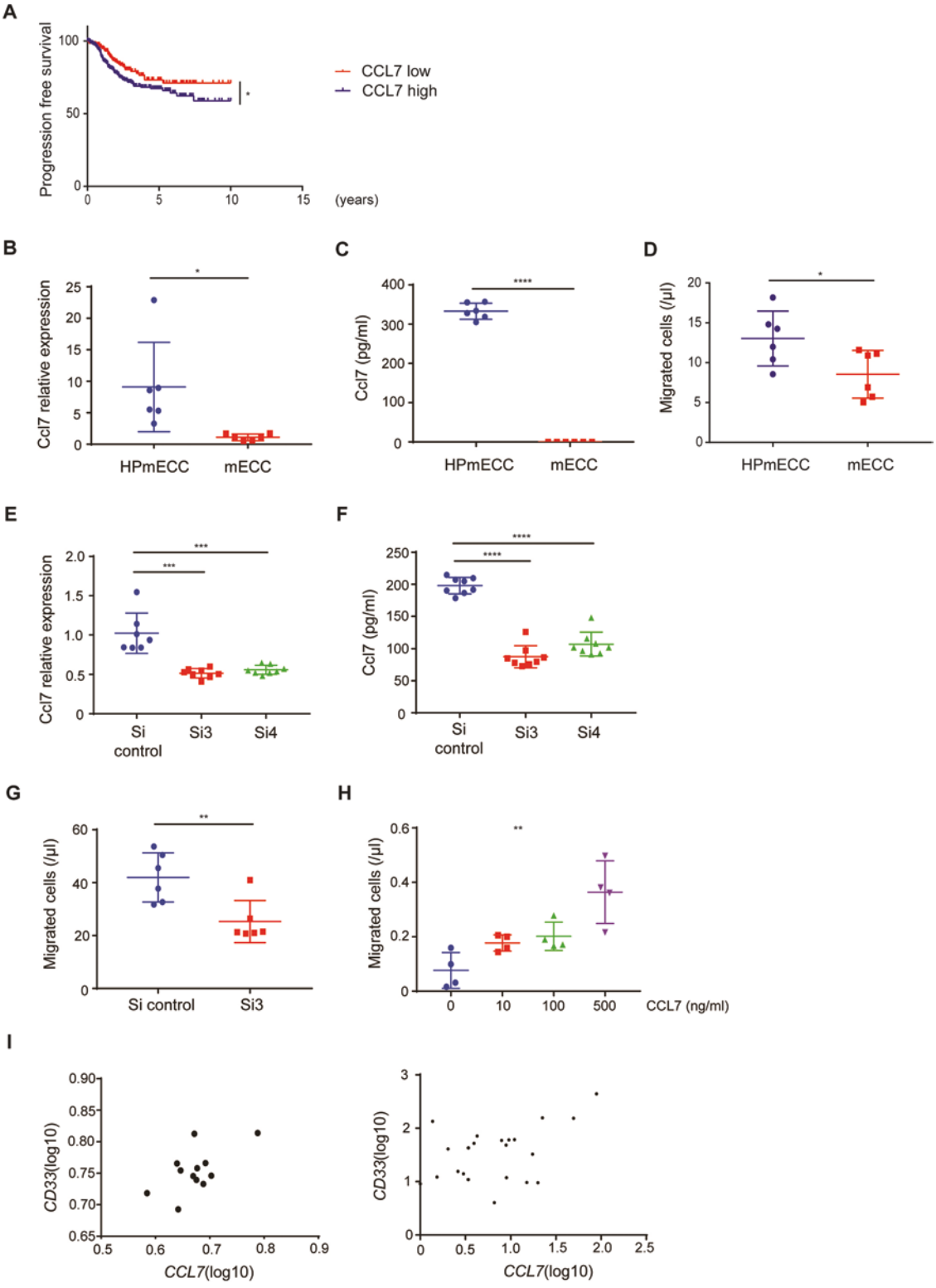

Figure 5. CCL7 secreted by HPmECCs promotes migration of MDSCs. (**A**) Survival analysis of TCGA endometrial cancer dataset along with CCL7 expression. Ten years progression free survival was compared between top one third group (CCL7 high) and bottom one third group (CCL7 low). *P = 0.0436, Log-rank test. (**B**) mRNA expression of *Ccl7* in HPmECCs and mECCs. n = 6, *P = 0.0205, t-test. (**C**) Concentration of CCL7 in cultured medium of HPmECCs and mECCs. n = 6, ****P < 0.0001, t-test. (**D**) Chemotaxis assay of MDSCs treated with conditioned medium of HPmECCs or mECCs. n = 6, *P = 0.0366, t-test. (**E**) mRNA expression of *Ccl7* in HPmECCs treated with CCL7 siRNA (si3, si4) or control. n = 8, ***P = 0.0001 (control vs si3), P = 0.0002 (control vs si4), t-test. (**F**) Concentration of CCL7 in cultured medium of HPmECCs treated with CCL7 siRNA (si3, si4) or control. n = 8, ****P < 0.0001, t-test. (**G**) Chemotaxis assay of MDSCs incubated with conditioned medium of HPmECCs treated with CCL7 siRNA (si3) of or control. n = 6, **P = 0.0076, t-test. (**H**) Chemotaxis assay of MDSCs treated with recombinant CCL7. n = 4, **P = 0.001, one-way ANOVA. Averaged data are presented as the mean ± SD. (**I**) Positive correlation between gene expressions of *CD33* and *CCL7* in USC. (Left) GSE56026, n = 12, Pearson r = 0.6227, P = 0.03. (Right) TCGA, n = 397, Pearson r = 0.1573, P = 0.0013.

tablishing murine models with Y.M. and Y.H. S.T., R.M. and N.M. contributed RNAseq analysis. All authors contributed to sample collection, data acquisition, manuscript editing and manuscript review.

Data availability

RNA sequencing data have been deposited at Gene Expression Omnibus with accession number 176257 (GSE176257). Sequencing coverage and quality statistics of RNA sequencing was described in Supplementary Table 3. All other data are freely available from the corresponding author upon reasonable request.

References

1. Javadian, P. et al. (2020) Endometrial carcinoma and its precursors. *Adv. Exp. Med. Biol.*, 1242, 59–72.
2. Howlader, N. et al. *SEER Cancer Statistics Review, 1975–2017*, National Cancer Institute, Bethesda, MD. https://seer.cancer.gov/csr/1975_2017/, based on November 2019 SEER data submission, posted to the SEER web site, April 2020.
3. Moore, K.N. et al. (2011) Uterine papillary serous carcinoma. *Clin. Obstet. Gynecol.*, 54, 278–291.
4. Holman, L.L. et al. (2017) Factors prognostic of survival in advanced-stage uterine serous carcinoma. *Gynecol. Oncol.*, 146, 27–33.
5. Kandoth, C. et al. (2013) Integrated genomic characterization of endometrial carcinoma. *Nature*, 497, 67–73.
6. Zhao, S. et al. (2013) Landscape of somatic single-nucleotide and copy-number mutations in uterine serous carcinoma. *Proc. Natl. Acad. Sci. USA*, 110, 2916–2921.
7. Zhang, L. et al. (2020) Pathogenesis and clinical management of uterine serous carcinoma. *Cancers (Basel)*, 12.
8. Kang, H.S. et al. (2011) GPR54 is a target for suppression of metastasis in endometrial cancer. *Mol. Cancer Ther.*, 10, 580–590.
9. Kharma, B. et al. (2013) Utilization of genomic signatures to identify high-efficacy candidate drugs for chemorefractory endometrial cancers. *Int. J. Cancer.*, 133, 2234–2244.
10. Kharma, B. et al. (2014) STAT1 drives tumor progression in serous papillary endometrial cancer. *Cancer Res.*, 74, 6519–6530.
11. Zeng, X. et al. (2019) Phosphorylation of STAT1 serine 727 enhances platinum resistance in uterine serous carcinoma. *Int. J. Cancer.*, 145, 1635–1647.
12. Binnewies, M. et al. (2018) Understanding the tumor immune microenvironment (TIME) for effective therapy. *Nat. Med.*, 24, 541–550.
13. Antomarchi, J. et al. (2019) Immunosuppressive tumor microenvironment status and histological grading of endometrial carcinoma. *Cancer Microenviron.*, 12, 169–179.
14. Hamanishi, J. et al. (2007) Programmed cell death 1 ligand 1 and tumor-infiltrating CD8+ T lymphocytes are prognostic factors of human ovarian cancer. *Proc. Natl. Acad. Sci. USA*, 104, 3360–3365.
15. Hamanishi, J. et al. (2011) The comprehensive assessment of local immune status of ovarian cancer by the clustering of multiple immune factors. *Clin. Immunol.*, 141, 338–347.
16. Li, K. et al. (2009) Clinical significance of the NKG2D ligands, MICA/B and ULBP2 in ovarian cancer: high expression of ULBP2 is an indicator of poor prognosis. *Cancer Immunol. Immunother.*, 58, 641–652.
17. Hamanishi, J. et al. (2015) Safety and antitumor activity of anti-PD-1 antibody, nivolumab, in patients with platinum-resistant ovarian cancer. *J. Clin. Oncol.*, 33, 4015–4022.
18. Peng, J. et al. (2015) Chemotherapy induces programmed cell death-ligand 1 overexpression via the nuclear factor-κB to foster an immunosuppressive tumor microenvironment in ovarian cancer. *Cancer Res.*, 75, 5034–5045.
19. Pakish, J.B. et al. (2017) Immune microenvironment in microsatellite-instable endometrial cancers: hereditary or sporadic origin matters. *Clin. Cancer Res.*, 23, 4473–4481.
20. Cai, Y. et al. (2019) Multi-omics profiling reveals distinct microenvironment characterization of endometrial cancer. *Biomed. Pharmacother.*, 118, 109244.
21. Musacchio, L. et al. (2020) Immunotherapy in endometrial cancer: rising choice for endometrial cancer patients? *J. Clin. Med.*, 9.
22. Mulati, K. et al. (2019) VISTA expressed in tumour cells regulates T cell function. *Br. J. Cancer.*, 120, 115–127.
23. Taki, M. et al. (2018) Snail promotes ovarian cancer progression by recruiting myeloid-derived suppressor cells via CXCR2 ligand upregulation. *Nat. Commun.*, 9, 1685.
24. Blaisdell, A. et al. (2015) Neutrophils oppose uterine epithelial carcinogenesis via debridement of hypoxic tumor cells. *Cancer Cell*, 28, 785–799.
25. Yamanoi, K. et al. (2016) Suppression of ABHD2, identified through a functional genomics screen, causes anoikis resistance, chemoresistance and poor prognosis in ovarian cancer. *Oncotarget*, 7, 47620–47636.
26. Solito, S. et al. (2019) Methods to measure MDSC immune suppressive activity in vitro and in vivo. *Curr. Protoc. Immunol.*, 124, e61.
27. Horikawa, N. et al. (2020) Anti-VEGF therapy resistance in ovarian cancer is caused by GM-CSF-induced myeloid-derived suppressor cell recruitment. *Br. J. Cancer*, 122, 778–788.
28. Felix, K. (2016). *Trim Galore*. http://www.bioinformatics.babraham.ac.uk/projects/trim_galore/ (20 March 2022, date last accessed).
29. Dobin, A. et al. (2013) STAR: ultrafast universal RNA-seq aligner. *Bioinformatics*, 29, 15–21.
30. Li, B. et al. (2011) RSEM: accurate transcript quantification from RNA-Seq data with or without a reference genome. *BMC Bioinf.*, 12, 323.
31. Daikoku, T. et al. (2008) Conditional loss of uterine Pten unfailingly and rapidly induces endometrial cancer in mice. *Cancer Res.*, 68, 5619–5627.
32. Li, B.L. et al. (2020) Prognostic significance of immune landscape in tumour microenvironment of endometrial cancer. *J. Cell. Mol. Med.*, 24, 7767–7777.
33. Cheng, P. et al. (2021) Bioinformatic profiling identifies prognosis-related genes in the immune microenvironment of endometrial carcinoma. *Sci. Rep.*, 15.
34. Kortlever, R.M. et al. (2017) Myc cooperates with Ras by programming inflammation and immune suppression. *Cell*, 171, 1301–1315.e14.
35. Casey, S.C. et al. (2016) MYC regulates the antitumor immune response through CD47 and PD-L1. *Science*, 352, 227–231.
36. Whitfield, J.R. et al. (2017) Strategies to inhibit Myc and their clinical applicability. *Front. Cell Dev. Biol.*, 5, 10.
37. Truica, M.I. et al. (2021) Turning up the heat on MYC: progress in small-molecule inhibitors. *Cancer Res.*, 81, 248–253.
38. Cheng, H. et al. (2014) A genetic mouse model of invasive endometrial cancer driven by concurrent loss of Pten and Lkb1 Is highly responsive to mTOR inhibition. *Cancer Res.*, 74, 15–23.
39. Fedorko, A.M. et al. (2020) An immune competent orthotopic model of endometrial cancer with metastasis. *Heliyon*, 6, e04075.
40. Tseng, S.H. et al. (2020) Novel, genetically induced mouse model that recapitulates the histological morphology and immunosuppressive tumor microenvironment of metastatic peritoneal carcinomatosis. *J. ImmunoTher. Cancer.*, 8, e000480.
41. Liu, Y. et al. (2018) Crucial biological functions of CCL7 in cancer. *PeerJ*, 6, e4928.
42. Hao, Q. et al. (2020) CCL2/CCR2 signaling in cancer pathogenesis. *Cell Commun. Signal.*, 18, 82.
43. Yang, H. et al. (2020) CCL2-CCR2 axis recruits tumor associated macrophages to induce immune evasion through PD-1 signaling in esophageal carcinogenesis. *Mol. Cancer*, 19, 41.
44. Lahmar, Q. et al. (2021) Monocytic myeloid-derived suppressor cells home to tumor-draining lymph nodes via CCR2 and locally modulate the immune response. *Cell. Immunol.*, 362, 104296.
45. Yuanyuan, L. et al. (2021) Myeloid NEMO deficiency promotes tumor immunosuppression partly via MCP1-CCR2 axis. *Exp. Cell Res.*, 399, 112467.
46. Teng, K.Y. et al. (2017) Blocking the CCL2-CCR2 axis using CCL2-neutralizing antibody is an effective therapy for hepatocellular cancer in a mouse model. *Mol. Cancer Ther.*, 16, 312–322.